Thyroid-stimulating hormone receptor signaling restores skeletal muscle stem cell regeneration in rats with muscular dystrophy

Valentina Taglietti, Kaouthar Kefi, Lea Rivera, Oriane Bergiers, Nastasia Cardone, Fanny Coulpier, Stamatia Gioftsidi, Bernadette Drayton-Libotte, Cyrielle Hou, François-Jérôme Authier, et al.

Sci. Transl. Med., 15 (685), eadd5275.
DOI: 10.1126/scitranslmed.add5275

View the article online
https://www.science.org/doi/10.1126/scitranslmed.add5275

ACCEPTED VERSION

Title: Thyroid-stimulating hormone receptor signaling restores skeletal muscle stem cell regeneration in rats with muscular dystrophy

Authors: Valentina Taglietti[1], Kaouthar Kefi[1], Lea Rivera[1], Oriane Bergiers[1], Nastasia Cardone[1], Fanny Coulpier[1], Stamatia Gioftsidi[1], Bernadette Drayton-Libotte[1], Cyrielle Hou[1], François-Jérôme Authier[1,2], France Pietri-Rouxel[3], Matthieu Robert[4,5], Dominique Bremond-Gignac[5,6], Claudio Bruno[7], Chiara Fiorillo[7], Edoardo Malfatti[1,2], Peggy Lafuste[1,10], Laurent Tiret[1,8,10], Frédéric Relaix[1,2,8,9,10,11*].

Affiliations:

1. Univ Paris-Est Créteil, INSERM, U955 IMRB, F-94010 Créteil, France

2. AP-HP, Hôpital Mondor, FHU SENEC, Service d'histologie, F-94010 Créteil, France

3. Sorbonne Université, INSERM, UMRS974, Center for Research in Myology, F-75013, Paris, France

4. Borelli centre, UMR 9010, CNRS - SSA - ENS Paris Saclay - Université Paris Cité, F-75016, Paris, France

5. Ophthalmology Department, Necker Enfants Malades University Hospital, AP-HP, F-75015, Paris, France

6. INSERM, UMRS1138, Team 17, Sorbonne Paris Cité University, Centre de Recherche des Cordeliers, F-75006, Paris, France

7. Center of Translational and Experimental Myology, IRCCS Gaslini Institute, DINOGMI, University of Genova, 16147, Genova, Italy

8. École nationale vétérinaire d'Alfort, IMRB, F-94700, Maisons-Alfort, France

9. EFS, IMRB, F-94010, Creteil, France
10. Senior authors
11. Lead Contact
*Correspondence: frederic.relaix@inserm.fr

OVERLINE: MUSCULAR DYSTROPHY

One Sentence Summary: The adenylyl cyclase activator forskolin improves muscle regeneration in dystrophic rats.

ABSTRACT

Duchenne muscular dystrophy (DMD) is a severe and progressive myopathy leading to motor and cardiorespiratory impairment. We analyzed samples from patients with DMD and a preclinical rat model of severe DMD and determined that compromised repair capacity of muscle stem cells in DMD is associated with early and progressive muscle stem cell senescence. We also found that extraocular muscles (EOMs), which are spared by the disease in patients, contain muscle stem cells with long-lasting regenerative potential. Using single-cell transcriptomics analysis of muscles from a rat model of DMD, we identified the gene encoding thyroid-stimulating hormone receptor (*Tshr*) as highly expressed in EOM stem cells. Further, TSHR activity was involved in preventing senescence. Forskolin, which activates signaling downstream of TSHR, was found to reduce senescence of skeletal muscle stem cells, increase stem cell regenerative potential, and promote myogenesis, thereby improving muscle function in DMD rats. These findings indicate that stimulation of adenylyl cyclase leads to muscle repair in DMD, potentially providing a therapeutic approach for patients with the disease.

INTRODUCTION

Duchenne muscular dystrophy (DMD) is a progressive skeletal muscle-wasting disorder caused by mutation in the *dystrophin* (*DMD*) gene, located on the X chromosome (*1*). DMD-causing mutations abolish the production of functional dystrophin. Dystrophin provides structural stability to the skeletal muscle, maintains muscle strength and flexibility, and protects the sarcolemma from contraction-induced injury (*2*). In patients with DMD, muscle fibers are damaged and undergo cycles of necrosis and repair, progressively leading to the failure of muscle regeneration. The deleterious remodeling of the dystrophic muscle is characterized by early interstitial fibrosis and infiltration of adipose cells within weakened and necrotic myofibers. In vertebrates, the robust capacity of muscle regeneration relies on the mobilization of quiescent muscle stem cells (MuSCs), also named satellite cells because of their specific position peripheral to the myofiber and intercalated under the extracellular matrix. Upon activation, MuSCs proliferate, then differentiate and fuse into new myofibers that reconstruct the damaged tissue, while maintaining a regenerative pool (*3*). These events involve the coordinated spatio-temporal interaction of growth factors, cytokines, and inflammatory mediators that are exchanged by infiltrating cells, MuSCs, and their cellular niche. The process provides a favorable environment for the efficient and lasting contribution of MuSCs to the muscle repair process. In DMD conditions, the integrity of these mechanisms is disrupted: Myonecrosis induces oxidative stress leading to the activation of pathways that induce early senescence of macrophages, MuSCs, and endothelial cells, resulting in chronic stimulation of inflammatory pathways and increased fibrosis within the affected muscle. The molecular mechanisms underlying this impairment are not fully deciphered.

The most frequent mutations in children with DMD occur between exons 45 and 55 of the *DMD* gene (*4*). To provide a preclinical model resembling this type of the disease, we generated an out-of-frame deletion of exon 52 in the rat *dystrophin* gene (R-DMDdel52). These rats

almost completely lacked dystrophin protein expression in skeletal and cardiac muscles, leading to a severe muscle dystrophy phenotype that mimics many aspects of the DMD condition in humans (*5*). Here, we showed that R-DMDdel52 animals display an early onset impairment of MuSC myogenic capacity, leading to a progressive reduction in muscle regenerative potential.

Extraocular muscles (EOMs) form a group of specialized muscles that consist of four recti (superior, medial, inferior, and lateral) and two oblique muscles (superior and inferior). EOMs are developmentally, anatomically, and physiologically distinct from other skeletal muscles. These muscles are spared in patients with DMD (*6,7*), suggesting either distinct requirements for dystrophin in these muscles or the presence of adaptative compensatory mechanisms. We confirmed that EOMs are spared and exhibit long-lasting regenerative capacity in this rat model. Comparative analysis of single-cell RNA sequencing (scRNA-seq) data from R-DMDdel52 rats and their wild-type littermates revealed broad molecular changes in cell populations of affected muscles (limb) versus spared muscles (EOMs) in DMD conditions. In MuSCs of limb muscles of the R-DMDdel52 rats, we quantified increased expression of senescence markers at the transcript or protein levels, such as P21 (encoded by *Cdkn1a*), P16 (encoded by *Cdkn2a*) (*8, 9*), and histone H2A gamma X (γH2AX) (*10-12*). This molecular signature, which was shared with patients with DMD, was absent in the EOMs of R-DMDdel52 rats.

Thyroid-stimulating hormone receptor (TSHR) is a G-protein-coupled receptor for thyrostimulin and thyroid-stimulating hormone (*13*). TSHR activation leads to the stimulation of adenylyl cyclase that produces the second messenger cyclic adenosine monophosphate (cAMP), which activates protein kinase A. *TSHR* transcripts are abundant in thyroid follicular cells (*14-15*). *TSHR* is also expressed in some extra-thyroid tissues and in some cancers (*16, 17*). Here, we showed that *TSHR* is also expressed in EOM MuSCs and that the TSHR pathway

regulates MuSCs senescence. We stimulated TSHR signaling in R-DMDdel52 rats using forskolin, an activator of adenylyl cyclase (*18*), and rescued the proliferation and differentiation defects observed in the MuSCs from DMD-affected limb muscles. Furthermore, we found that forskolin treatment reversed senescence of DMD MuSCs, promoting skeletal muscle tissue repair and improving performance of DMD muscle function.

RESULTS

Extraocular muscles retain muscle regenerative capacity in R-DMDdel52 rats

Using the CRISPR/Cas9 system, we generated DMD rats with specific deletion of 188 bp of exon 52 in the *Dmd* gene (R-DMDdel52) (*5*). Limb skeletal muscles of R-DMDdel52 rats displayed features of severe muscle dystrophy including altered fiber morphology, invading inflammatory cells, and endomysial fibrosis (Fig. 1A). Quantification of acute fibrotic deposition, by measuring the percentage of area occupied by connective tissue detected with Sirius red staining, showed a significant increase in R-DMDdel52 in tibialis anterior (TA) compared to that of TA from their wild-type littermates (Fig. 1B; $P = 0.001$).

Because EOMs are selectively spared in DMD (*6, 7*), we performed histological analyses on the global layer of recti and oblique EOMs; we did not study retractor bulbi and levator palpebrae superioris (Fig. S1A-C). We analyzed the global layer because regenerating myofibers are scarce in this region in the healthy condition (*19-25*). Hematoxylin and eosin (H&E) and Sirius red staining confirmed sparing of EOMs isolated from 12-month-old R-DMDdel52 animals (Fig. 1C), as indicated by the lack of inflammation or fibrosis compared to wild-type controls (Fig. 1C-D). Thus, R-DMDdel52 rats displayed the general histopathological features of severe muscular dystrophy of patients with DMD, as well as the sparing of EOMs, reinforcing the predictive value of this rodent model.

We assessed the time course of muscle regeneration of R-DMDdel52 TA. Transverse sections were immunostained for embryonic myosin heavy chain (eMHC), a specific marker of developmental and regenerating myofibers. At 3 weeks of age, eMHC-positive myofibers were absent in wild-type TA but were abundant in R-DMDdel52 TA (Fig. 1E). The number of regenerating fibers in R-DMDdel52 rats decreased markedly during the first year of life (Fig. 1E-F), suggesting that progressively impaired capacity for muscle regeneration is associated

with disease progression. By contrast, we observed that the regenerative process in EOMs occurs to a lesser extent, compared to that in early pathological states in limb muscle, and remained stable between 3 weeks and 12 months of age (Fig. 1G-H). These data suggested that EOMs maintain their regenerative capacity over time in DMD conditions.

Because the regenerative capacity of skeletal muscles depends on the renewal and activation properties of MuSCs, we quantified their number and myogenic status in TA or EOMs from wild-type and R-DMDdel52 rats by co-immunostaining for PAX7, a marker of MuSCs, and Ki67, a marker of proliferation. We observed no differences in the number of MuSCs per fiber (based on quantification of PAX7-positive cells) between wildtype and R-DMDdel52 in either TA or EOMs (Fig. 1I-M), rejecting the hypothesis that MuSCs are lost during DMD progression. Next, we observed that nearly half of the MuSC pool proliferated in the growing 3-week-old TA of both R-DMDdel52 and wild-type rats and that these cells then exited the cell cycle at later ages (Fig. 1I-K). By contrast, a majority of MuSCs in EOMs remained positive for Ki67 in R-DMDdel52 rats throughout the first year (Fig. 1L-N), suggesting that the capacity of regeneration of these muscles during this time is based on a stable pool of stem cells that self-renew.

MuSC-derived myoblasts from R-DMDdel52 rat limbs display impaired myogenic potential in vitro

To compare change in intrinsic myogenic properties of wild-type or dystrophin-deficient myoblasts originating from limb or EOM MuSCs, we isolated muscle cells by mechanical and enzymatic dissociation of bulk TA and EOMs, sampled from 3-week- and 6-month-old wild-type and R-DMDdel52 animals. MuSCs in culture activated into myoblasts in proliferation medium, then matured and fused into myotubes in a differentiation medium (see Methods). MuSCs isolated from 3-week-old animals from either muscle type or genotype exhibited

similar proliferation (Ki67 positivity), and myogenic differentiation (myotube formation) capacities (Fig. 2A-F). However, MuSCs isolated from TA of 6-month-old DMD rats showed a strong decrease in their capacity for activation and proliferation (Fig. 2G), whereas those from EOMs from these animals retained these capacities (Fig. 2H-L). Moreover, cultured TA MuSCs from the DMD rats displayed a marked reduction in their capacity to fuse compared with cells from wild-type rat TA or EOMs from either genotype (Fig. 2J-K). The reduced fusion resulted in a decrease in the number of nuclei per myotube formed by MuSCs from TA from DMD rats compared to those from TA from wild-type rats (Fig. 2L). Conversely, DMD and wild-type myoblasts isolated from EOMs differentiated at the same rate and to the same extent (Fig.2J-L). These data suggested that EOM MuSCs from DMD rats retained their myogenic potential ex vivo.

To evaluate whether the proliferation and differentiation impairments that we observed in MuSC-derived myoblasts cultured from TA of R-DMDdel52 rats are cell autonomous, we used fluorescence-activated cell sorting (FACS) to isolate pure populations of MuSCs from limb muscles (Fig. S2A). Purity of the cell population was confirmed after 48 hours of culture with >90% of the population positive for either PAX7 or MYOD (or both) (Fig. 2M-N). We found that the sorted MuSCs from the limb muscles of R-DMDdel52 rats proliferated less (Fig. 2O), differentiated poorly, and had limited fusion capacity when compared with MuSCs isolated from limb muscles of wild-type rats (Fig. 2P-Q). Most of the unfused nuclei from the R-DMDdel52 limb muscles were PAX7 and/or myogenin-positive, indicating that R-DMDdel52 myoblasts failed to fuse (Fig. S2B). In addition, the sorted MuSCs prepared from EOMs of R-DMDdel52 rats aged 6 months did not show any proliferation or differentiation defects compared to sorted MuSCs prepared from EOMs from wild-type rats, suggesting that EOM MuSCs are intrinsically spared (Fig. S2C-G). We concluded that EOM MuSCs of R-

DMDdel52 rats are protected against the myogenic potential loss observed in limb muscles MuSCs.

Limb muscle satellite cells of R-DMDdel52 rats acquire an early signature of senescence.

To investigate the molecular and cellular changes underlying the differential myogenic potential of MuSCs in R-DMDdel52 rats, we analyzed single-cell transcriptomes (scRNA-seq) from TA of 12-month-old R-DMDdel52 and their wild-type littermates. Cells were extracted by enzymatic and mechanical digestion, and vital cells were selected by FACS to remove dead cells, aggregated cells, and debris. We performed scRNA-seq using the 10x Genomic Chromium and Illumina NextSeq 550 system. Cells were filtered based on reads per sample, mitochondrial and ribosomal RNA content, and predicted doublets by cell barcode selection, to yield an average of 6247 cells per sample (Table 1). Cell identities were assessed based on previously established markers (*26*). Data were visualized by t-distributed stochastic neighborhood embedding (t-SNE). We identified 9 major clusters of muscle-resident cells (Fig. 3A). Wild-type and R-DMDdel52 cells were color-labelled on the t-SNE map, which highlighted disease-related changes at the whole-transcriptome level (Fig. 3B). These changes were prominent for MuSCs, which showed distinct gene expression signatures between wild-type and R-DMDdel52 samples. In TA, we found that genes encoding cyclin-dependent kinase inhibitors P21 (*Cdkn1a*) and P16 (*Cdkn2a*, also referred to as *p16Ink4a*), which are markers of growth arrest markers (*8*), were induced in R-DMDdel52 MuSCs when compared to controls (Fig. 3B). We validated that this transcriptional activation resulted in increased protein specifically in R-DMDdel52 MuSCs by immunostaining for P16 or P21 and PAX7 in TA from rats 12 months of age (Fig.3C-D). We also observed a higher presence of the phosphorylated form of γH2AX, a marker of DNA damage induced in senescent cells (*10-12*) in TA MuSCs of R-DMDdel52 compared to wildtype (Fig. 3E). We evaluated the presence of this senescence

signature during disease progression (Fig. 3F-H). As early as 3 weeks of age and increasingly over time, a majority of MuSCs in limb muscle of R-DMDdel52 rats acquired a senescent phenotype, in contrast to wild-type MuSCs (Fig. 3F-H). This senescence trajectory was consistent with the progressive waning of muscle regenerative potential and with the phenotype observed ex vivo in MuSC cultures.

Given the sparing of EOMs from regenerative decline in DMD, we investigated the transcriptome of EOM satellite cells using scRNA-seq. We analyzed transcriptomes of an average of 2505 cells (Fig. 3I) and confirmed, in both wild-type and R-DMDdel52 EOM MuSCs, the positional identity of activated *Pax7*+/*Myf5*+ MuSCs by the high expression of *Pitx2* (*27, 28*) (Fig. 3, I and J). In MuSCs from R-DMDdel52 EOMs, we detected a very low amount of *Cdkn1a* transcripts, and *Cdkn2a* transcripts were almost undetectable (Fig. 3J). We confirmed these data by RT-qPCR on MuSCs freshly isolated from EOMs (Fig. 3K). Immunostaining on sections of R-DMDdel52 and wild-type EOMs for PAX7 and P16, P21, or γH2AX revealed that none of the PAX7-positive cells were positive for P16 (fig. S3A) and only a small percentage of these PAX7-positive cells were positive for γH2AX and P21 (fig. S3, B to E) with no differences between the R-DMDdel52 and wild-type samples. Altogether, these data demonstrated that MuSCs from DMD-affected and DMD-spared muscles have a different status that is associated with unique transcriptional profiles. Furthermore, we established an association between the status of the DMD-affected muscle and a molecular signature of MuSC senescence. We therefore proposed that early senescence of MuSCs is a central mechanism for the early and progressive loss of muscle regenerative potential.

TSHR signaling controls senescence in myoblasts isolated from EOMs from R-DMDdel52 rats

In addition to *Pitx2*, EOM MuSCs also specifically expressed *Tshr*, encoding the receptor for thyroid-stimulating hormone (Fig. 3, I to K). We validated the higher amount of TSHR protein

in EOM MuSCs by performing immunofluorescence on freshly isolated myogenic cells from EOMs and limb muscles. TSHR was abundant in EOM-derived myoblasts, whereas it was barely detectable in myoblasts isolated from limb muscles (Fig. 4A). To assess the functional relevance of TSHR in EOM MuSCs, we treated myoblasts isolated by mechanical and enzymatic dissociation of wild-type EOMs with a selective TSH receptor inverse agonist, ML224 (*29*). Inhibition of TSHR signaling compromised myoblast proliferation as indicated by a decrease in PAX7:$MYOD^{+}/EdU^{+}$ cells compared to cells treated with the vehicle (Fig. 4, B and C). The effects of TSHR inhibition by ML224 were reversed by the treatment with forskolin, a well-known activator of adenylyl cyclase (*18*) (Fig. 4, B and C). Furthermore, cultured EOM MuSC cells treated with TSHR inhibitor showed increased expression of *Cdkn1a* and *Cdkn2a* (Fig. 4D), suggesting the acquisition of a senescence signature (*30*). Forskolin also prevented the increase in *Cdkn1a* and *Cdkn2a* expression induced by ML224 (Fig. 4D), indicating that forskolin protected MuSCs from entering into senescence. In addition, EOM myoblasts treated with ML224 displayed differentiation defects and compromised myotube formation, associated with a reduction in the fusion index compared to control cells (Fig. 4, E to G). Forskolin also protected the fusion capacity of differentiated MuSCs such that in EOM-derived myoblasts the fusion index and nuclei per myotube of cells treated with forskolin and ML222 were similar that those of control cells (Fig. 4F-G). ML224-treated EOM myoblasts showed proliferation and fusion capacities similar to those of cultured R-DMDdel52 limb-derived myoblasts (Fig 2J-Q), and these phenotypes could be rescued by forskolin treatment. Altogether, these data indicated that TSHR signaling through adenylyl cyclase prevents entry into senescence and maintains the myogenic potential of R-DMDdel52 EOM-derived MuSCs.

We evaluated whether stimulating adenylyl cyclase protects MuSC-derived myoblasts from limb muscles of R-DMDdel52 rats from precocious entry into senescence. We treated wild-

type and R-DMDdel52 MuSCs isolated from limb muscles with forskolin. Forskolin-treated R-DMDdel52 myoblasts exhibited increased proliferation compared to control R-DMDdel52 cells, reaching wild-type proliferative capacity (Fig. 4H-I). Furthermore, forskolin abolished the overexpression of *Cdkn1a* (p21) and *Cdkn2a* (p16) in R-DMDdel52 myoblasts, whereas R-DMDdel52 myoblasts treated with vehicle maintained high expression of these senescence markers (Fig. 4J). R-DMDdel52 limb myoblasts treated with forskolin also exhibited an improved differentiation potential compared to control R-DMDdel52 cells, forming larger myotubes with a higher fusion index (Fig. 4K-L). These data demonstrated that activation of the cAMP pathway delays MuSC senescence, rescuing both the proliferation and differentiation defects observed in R-DMDdel52 myoblasts.

Progressive loss of tissue repair in human DMD is associated with a MuSC-specific senescence signature

To confirm the findings from our rat model in humans, we analyzed regeneration and senescence in deltoid muscle biopsies obtained from patients with DMD and age-matched non-DMD controls. Muscle biopsies were sorted by age classes and regenerating myofibers were identified by eMHC staining (Fig. 5A). Quantification of eMHC-positive myofibers highlighted an early age and abrupt decline in muscle regeneration capacity (Fig. 5B), consistent with data obtained in the rat model (Fig. 1E-H). To evaluate the senescence status of human muscle stem cells, we performed immunostaining for PAX7 with P16 or γH2AX on sections from DMD and control biopsies (Fig. 5C-D). Compared to controls, muscle sections from patients with DMD exhibited a substantial number of PAX7-positive MuSCs that co-expressed P16 (Fig. 5E) or γH2AX (Fig.5F). Thus, we concluded that MuSCs of patients with DMD display an early senescent signature, associated with a gradual decline of muscle regenerative potential.

To assess the predictive value of molecular mechanism identified in R-DMDdel52 model, we evaluated *TSHR* expression in human myoblasts isolated from human deltoid muscles and EOMs of non-myopathic controls. Both transcript analysis and immunofluorescence analysis revealed robust expression of TSHR in myoblasts isolated from human EOMs compared to the that in myoblasts isolated from limb control muscles (Fig. 5G-H). Accordingly, treatment of human EOM myoblasts with ML224 caused a decreased proliferation rate specifically in EOM myoblasts and not in limb myoblasts (Fig. 5I-L). These data validated the endogenous presence of TSHR on human EOM myoblasts and revealed a conserved functional role for TSHR in promoting myogenesis.

Systemic administration of forskolin to R-DMDdel52 rats increases muscle regeneration and functional performance

Having showed that in rats and humans modulation of the TSHR pathway impacts the regenerative potential of muscle stem cells, we assessed the therapeutic relevance for DMD of a TSHR pathway agonist in vivo. We performed intraperitoneal administration of 2.5 mg/kg of forskolin or vehicle twice a week in one-month-old R-DMDdel52 and wild-type rats for 2 months, performing functional evaluations every 4 weeks and killing these animals at four months of age (Fig. 6A).

To establish a functional baseline, we performed forelimb grip tests every month starting at 4 weeks of age, before the first injection. During the course of evaluation, R-DMDdel52 animals showed progressive decreased muscle force compared to wildtype (Fig. 6B). Forskolin-treated R-DMDdel52 animals performed better than those treated with only vehicle after two months of treatment (Fig. 6B). To evaluate whether a 2-month treatment with forskolin also led to a beneficial effect on the overall capacity to sustain physical exercise, we gradually acclimated the rats to running on a treadmill and measured the time of exhaustion during a run at a

gradually increased imposed speed. R-DMDdel52 rats treated with forskolin ran longer than R-DMDdel52 rats treated with vehicle (Fig. 6C). No differences were observed between forskolin-treated and vehicle-treated wild-type rats in the functional tests performed.

Using H&E staining, we evaluated muscle histology of TA transverse sections in animals at the end of the treatment period. The results confirmed the safety of forskolin on skeletal muscle: images of forskolin-treated wild-type rats were indistinguishable from those of wild-type rats treated with the vehicle (Fig.6D). Although we observed no restoration of the myofiber diameter in forskolin-treated R-DMDdel52 rats compared to genotype-matched vehicle-treated rats (Fig. 6E), we found reduced fibrotic remodeling quantified by the area of the Sirius red (Fig. 6, F and G). The amelioration of histological pathology by forskolin administration was accompanied by a marked increase in myofiber regeneration as indicated by eMHC positivity (Fig. 6, H and I) and a higher number of proliferating $Ki67^{+}$ MuSCs (Fig. 6, J and K). We also observed a lower percentage of PAX7-positive MuSCs that were also positive for the senescence marker P16 in R-DMDdel52 rats after forskolin administration, supporting the protective role of forskolin in reducing the acquisition of a senescence state in vivo (Fig. 6, L and M). Finally, MuSC-derived myoblasts isolated from quadriceps of forskolin-treated R-DMDdel52 rats displayed higher proliferative and differentiation capacities in vitro (Fig. 6, N to Q), compared to control cells isolated from vehicle-treated R-DMDdel52 rats. Consistent with high activity of TSHR signaling in EOMs, no changes were observed in myoblasts isolated from the EOMs of wild-type and R-DMDdel52 rats treated with forskolin or only vehicle (fig. S4, A to D).

DISCUSSION

DMD is an early disabling and fatal disease, necessitating the identification of innovative therapeutic options that could at least modify the trajectory of the disease to offer patients and their families the potential for autonomy and improvement in quality of life. The DMD rat model used here was generated by genome editing and is the first rat model carrying a mutation analogous to the region between exons 45 and 55 of human *DMD*, where the majority of mutations in children are found (*31*). Previously, we established that the severity and evolution of the disease closely mimics the situation of patients, including mortality earlier than half of the normal life expectancy of the animals (*5*). We reinforce here the relevance of this model by reporting the absence of important abnormalities in EOMs, which, as in patients with DMD, are spared from the progressive loss of muscle repair observed in other skeletal muscles.

We showed that in contrast to limb muscles, EOMs of R-DMDdel52 rats retain regeneration capacity that could be explained by the superior expansion ability of their MuSCs, which exhibited, as previously reported (*32*), greater proliferation, differentiation, and self-renewal than their limb and diaphragm counterparts. Whereas the sparing of EOMs has been known for years, the molecular mechanisms underlying increased regenerative potential of the EOMs remained unknown. Using a large-scale analysis of all muscle cells, we revealed a MuSC-specific transcriptomic signature, confirmed at the protein level, of progressive senescence of limb MuSCs in our R-DMDdel52 rats, as well as in patients with DMD. Furthermore, this signature differed from that of the EOM MuSCs that are protected from this precocious senescence process. Senescence is also detected in macrophages, and endothelial cells of the DMD limb muscle (*33, 34*); thus appearing to be a key mechanism for the deviation of an efficient physiological process of muscle repair to a morbid trajectory.

We demonstrated here that the regenerative capacity of a muscle is inversely correlated to the number of MuSCs expressing senescence markers rather than to the total number of MuSCs,

suggesting that the ratio of PAX7$^+$ cells negative for senescence markers may be a useful addition to the list of quantified biomarkers for evaluating innovative therapies. Indeed, a key feature of cellular senescence is permanent cell cycle arrest (*35*) that could explain the impairment of muscle regeneration independently from the maintenance of satellite cell numbers. We also showed that the high expression of TSHR transcript and protein is a specific signature of EOM MuSCs in rat and human samples, confirming previous data reporting TSHR protein expression in EOM myoblasts (*36*). In both patient samples and our rat model, inhibition of the TSHR pathway in muscle precursors of EOMs lowered their proliferative capacity, whereas stimulation of a pathway activated by TSHR signaling was sufficient to inhibit the expression of the *Cdkn1a* and *Cdkn2a* senescence markers and hence to increase proliferative, differentiation, and fusion capacities of limb muscle precursors. The R-DMDdel52 rat model thus confirmed the possible co-existence within a single individual of affected and spared muscles, providing robust in vivo evidence for the possibility to preserve long-lasting muscle function in an individual with DMD.

We also analyzed the effect of forskolin, a natural diterpenoid that increases cAMP production and mimics TSHR signaling (*37*), in vivo using the R-DMDdel52 rats with an emphasis on its role in protecting MuSCs from senescence, enhancing their activation, and promoting muscle repair. Importantly, the effects of forskolin have been evaluated in different diseases, such as cystic fibrosis, asthma, obesity, and glaucoma, without major side effects [reviewed in (*38*)]. We provide here proof of concept that forskolin treatment delayed the early onset of senescence of MuSCs and enhanced muscle regeneration in DMD conditions. The treatment had a beneficial impact through the reduction of fibrotic muscle remodeling and, more importantly, on both muscle strength and locomotor performance, highlighting the clinical importance of preventing DMD stem cell senescence. Furthermore, the R-DMDdel52 rat model allowed us to demonstrate that activation of the TSHR pathway by forskolin protects MuSCs from

senescence, independently from factors such as inter-individual variability, modifying genes, or environmental parameters, which are usually difficult to exclude in human populations.

Senescence of MuSCs can be abrogated by genetic *p16* silencing (*39, 40*) or by overexpression of *Atg7*, which is essential to induce autophagy (*41*). However, no pharmacological treatment effectively reverses senescence in skeletal muscle satellite cells. Here, we showed that senescence of MuSCs is prevented by a pharmacological treatment using forskolin. Forskolin is currently mainly used to treat metabolic syndrome and obesity (*42, 43*). The safety of forskolin treatment was demonstrated in several studies, with only minor and reversible adverse gastrointestinal events reported (*44, 45*). Although the high tolerability of forskolin has been demonstrated, our study provides only a proof of principle for a pathophysiologically relevant mechanism mediated by TSHR that could be modulated to improve muscle regeneration in DMD. Our in vivo approach was designed to confirm efficacy of forskolin in counteracting the senescence of MuSCs in the complex context of DMD muscle remodeled by the disease. In this condition, forskolin treatment indeed reduced MuSCs senescence and supported their differentiation and fusion capacity, ultimately promoting muscle repair and strength. This encouraging result is associated with a possible limitation that we need to explore in the long term. Indeed, forskolin stimulates adenylyl cyclase, which is widely distributed in different cell types and physiologically activated by a large number of paracrine neurotransmitters and humoral factors. For this reason, our study, which extends the already existing spectrum of therapeutic use of adenyl cyclase modifiers, constitutes a first step towards the exhaustive analysis of long-term benefits and the necessary optimization of the dosing regimen to avoid the occurrence of adverse systemic effects. In summary, this work highlights the therapeutic benefit of inhibiting stem cell senescence to promote tissue repair and paves the way for replicative studies in muscle and any other organ affected by an early loss of the regenerative potential of its stem cells.

Material and Methods

Study design

This study was designed to investigate the contribution of MuSCs in DMD progression in a newly generated DMD rat model (R-DMDdel52) and in samples from DMD patients. We evaluated MuSCs in or isolated from TA and EOM as muscles that exhibited dystrophy and were spared from dystrophy, respectively, in the rat model using male animals only. We used P16, P21, and γH2AX as markers of senescence, eMHC as a marker of developmental and regenerating myofibers, PAX7 as a marker of MuSC activation, Ki67 as a marker of proliferation, and MYOD and myotube formation as markers of myogenic differentiation. Using scRNA-seq of cells from R-DMDdel52 rats, we identified *Tshr* as highly expressed in EOM MuSCs, and we established the role of TSHR in protecting against the entry into senescence using in vitro and in vivo studies. To mimic TSHR signaling, we treated R-DMDdel52 rats with forskolin and evaluated MuSC activation, muscle regeneration, and motor function by grip strength and walking (treadmill) tests. Each experiment was performed at least in biological triplicate. Rats were randomly assigned to experimental groups. We evaluated muscle regeneration potential and MuSC senescence in DMD and control human biopsies. Patients' parents gave informed consent including a specific authorization for the utilization of the biopsy for research purposes. This study was conducted in accordance with the Declaration of Helsinki. Muscle samples were obtained in Italy. EOM samples were obtained from muscle resections performed as part of strabismus corrective surgeries performed in France. The analyses were conducted at Mondor Hospital and received authorization from the French local human ethics board, following current French legislation and hospital ethics committee (Approval #12-2009 at CPP Ile-de-France IX). As far as the nature of the experiment allowed, the evaluators were blinded.

Generation of R-DMDdel52 rats

The R-DMDdel52 line was generated by using CRISPR-Cas9 system to induce a deletion of exon 52 in the *Dystrophin* gene of Sprague Dawley rats *(5)*. Rats were housed in a pathogen-free facility with 12-h light and 12-h dark cycles in accordance with European Directive 2010/63/EU. To avoid putative interference with environmental confounding factors, both wild-type and DMD rats were littermates. DNA was PCR-amplified to determine the genotype of rats, using the following primers that span the exon 52 deletion mutational site: For 5'-CTAACGCATTTAAAATATGCTGTCA-3', Rev 5'-GTTGGCTTAGCTCAACAACCAAGAT-3'. All the procedures including animal handling were validated by the local Ethical committee registered under n°16, and approved by the French ministry of Research under n° APAFIS#25606-202005311746599 and APAFIS#31740-2021051920188358.

Forskolin in vivo treatment

Four-week-old wild-type and R-DMDdel52 rats were treated with 2.5 mg/kg forskolin (Sigma-Aldrich, F6886) dissolved in 5% dimethyl-sulfoxide (DMSO) or with 5% DMSO (vehicle). Forskolin or vehicle were injected intraperitoneally twice a week for 2 months.

Hematoxylin and eosin staining

After isolation, muscles were immediately frozen in isopentane cooled in liquid nitrogen and sectioned at 7 μm. Slides were dipped in Mayer's hematoxylin (Sigma-Aldrich) for 3 min and then in lithium carbonate solution for 3 s, followed by incubation in eosin for 30 s. After a wash, slides were dipped in 50% EtOH, then 70% EtOH, followed by equilibration in 95% and 100% EtOH . Slides were mounted with Eurokitt.

Sirius red staining

Slides were defrosted for 20 min at room temperature and dipped in 90% EtOH for 2 min and then for 25 min in picro-sirius red solution (Sigma-Aldrich). The slides were extensively washed and dehydrated in EtOH 100%. After clearing in xylene, slides were mounted in Eurokitt.

Immunohistochemistry on cryosections

Fresh frozen muscles were sectioned with the cryostat Leica CM3050S (Leica Biosystems) at 7 μm of thickness on Super Frost Plus slides (Thermo Fisher Scientific, 10149870). For cryo-sectioning, we trimmed the muscle surface by discarding 20 sections per cut and adjusted the orientation to obtain transversal sections before cutting each muscle throughout its length, . Slides were then stored at -80 °C until use. For staining, slides were defrosted and fixed with 4% paraformaldehyde (PFA) for 10 min at 4 °C. After washes in phosphate-buffered saline (PBS, pH 7.4), slides were placed in cold acetone:methanol (1:1) solution for 6 min at -20 °C and then incubated with 10% bovine serum albumin for 1 h. Primary antibodies were incubated overnight at 4 °C. The following primary antibodies targeting the indicated proteins were used: PAX7 (Santa Cruz Biotechnology, AB_2159836), Ki67 (Abcam, AB_302459), P16 (Abcam, AB_10858268), P21 (Thermofisher, AB_2890980), and γH2AX (Abcam, AB_297813). After repetitive washes, slides were incubated with secondary antibodies for 45 min at room temperature. Laminin staining was performed after the secondary antibody incubation, for 1 h at 37 °C using a conjugated antibody (Abcam, AB_2891039). Nuclei were counterstained with Hoechst (Sigma-Aldrich, B2261). Fluorescence was analyzed with LSM800 confocal. eMHC (Abcam, AB_670121) staining was performed without fixation and with permeabilization in 0.5% Triton in PBS for 5 min.

Analysis of EOMs

EOMs were enucleated with the eyeball and frozen in chilled isopentane. For each rat, 3 to 4 sections of EOMs were cut and at least three EOMs were analyzed in each experiment. All histological quantitative morphometric analyses were performed specifically on the global layer of the four recti muscles (Fig. S1B-C) and on the whole section area of oblique muscles.

Cell culture

Rat adult TA, hindlimb muscles, and EOMs were dissected and digested with 3 U/ml Dispase II (Roche, 4942078001) and 0.5 U/ml Collagenase A (Roche, 10103586001) for 1 h in Hepes-buffered saline solution (HBSS, pH 7.3) at 37 °C with gentle rocking. Cell suspension was passed through cell strainers and centrifuged 600 *g* for 5 min at 4 °C. The supernatant was discarded, and the cell pellet was resuspended in 20% fetal bovine serum (FBS, Cat#S1810-500 Dominique Dutscher) in DMEM (Cat#41966-029 Gibco) supplemented with 25 ng/ml bFGF (RP4037, Sigma-Aldrich), and penicillin/streptomycin 100 mg/ml. Cells were plated on Matrigel (354234, Life Sciences)-coated 8-chamber slides (Sarstedt, #94.6140.802). The cells were left for 48 h after which proliferation was assessed. After 48 h of proliferation, cells were cultured for 5 days in 5% FBS to induce differentiation.

Human EOMs and deltoid biopsies were dissociated with Pronase (1.5 mg/ml; P5147-5G Sigma-Aldrich) in DMEM at 37 °C for 20 min and passed through a cell strainer. Cells were centrifugated 20 min at 600g and seeded onto gelatin-coated flasks in F12 medium (Life Technologies, Gibco® 31765-027) with 20% FBS (Dutscher; CAT S1810-500), 0.2% Vitamines (MEM Vitamin Solution, Thermo Fisher Scientific; CAT 11120052), 1% MEM Non-Essential Amino Acids Solution, and 1% Penicillin-Streptomycin. MuSC-derived myoblasts were treated with 10 μM ML224 (HY12381-S, CliniSciences) for 2 days (and then assessed for proliferation) or 7 days (and then assessed differentiation). Where indicated,

myoblasts were exposed to 20 μM forskolin (F3917, Sigma-Aldrich) for 48 h from the plating. ML224 treatments were conducted in serum-free condition to avoid any stimulation of TSHR by TSH in the serum. Control cells were treated with DMSO (D8418, Sigma-Aldrich) as vehicle for ML224 and forskolin.

Proliferation was measured after 24 h in culture by adding to the culture medium a pulse of 10 mM 5-ethynyl-20-deoxyuridine (EdU) for 24 h (EdU Click-iT PLUS Kit C10640, Life Technologies). The fusion capacity of cultured cells was quantified by a fusion index calculated as the number of nuclei present in myotubes divided by the total number of nuclei.

FACS of MuSCs

After dissociation of cells from hindlimb muscle, cells were incubated with CD45-PE-Cy7 (BD Pharmingen, 552848), Ter119-PE-Cy7 (BD Pharmingen, 557853), CD31-PE-Cy7 (BD Pharmingen, 561410), and α7-integrin-FITC (CliniSciences, C179570-100) for 45 min at 4 °C. After washes with HBSS (pH 7.3) supplemented with DNase (Sigma-Aldrich, DN25), cells were sorted with a FacsAria (BD Pharmingen). MuSC population was identified as CD45:Ter119:CD31-negative and α7-integrin-positive. For EOM MuSCs, muscles of two distinct rats were pooled and assessed as in triplicate.

Immunofluorescence of cultured cells

Cells were fixed with 4% PFA for 10 min at 4 °C and permeabilized with 0.5% Triton for 6 min. After blocking with 10% BSA, cells were incubated overnight at 4 °C with the following primary antibodies targeting: PAX7 (Santa Cruz Biotechnology, AB_2159836), MYOD (Dako, clone 5.8A, M3512), Ki67 (Abcam, AB_302459), light meromyosin [the rod-like tail region of myosin heavy chain (MHC) (MF20, DSHB, AB_2147781). For TSHR staining, cells

were permeabilized for 5 min with 0.1% Triton in PBS and then incubated overnight with TSHR antibody (CliniSciences, AB_10856516). Cells were washed in PBS and incubated with secondary antibodies for 45 min at room temperature. Finally, nuclei were counterstained with Hoechst (Sigma-Aldrich, B2261). Fluorescence was analyzed with a LSM800 confocal.

RNA isolation and RT–qPCR

RNA was extracted using RNAqueous-Micro Total RNA Isolation Kit (Invitrogen) and retrotranscribed using SuperScript™ III Reverse Transcriptase (Invitrogen, 18080093) according to manufacturer's instructions. qPCR was performed using StepOnePlus real-time PCR system (Applied Biosystems) and SYBR Green detection tools. Results are reported as relative gene expression (2-DDCT) using vehicle-treated cells or EOM-derived myoblasts as reference. Gene expression for rat transcript was normalized to expression of *Actb* (encoding β-actin). The sequences of primers are the following: Rat *Cdkn1a* (For TGGACAGTGAGCAGTTGAGC, Rev ACACGCTCCCAGACGTAGTT); Rat *Tshr* (For CTTTGTCCTGTTCGTCCTGC, Rev AGTGAAGGGACTAGCATTGTC); Rat *Cdkn2A* (For TGCAGATAGACTAGCCAAGGGC, Rev CTCGCAGTTCGAATCTGCAC); *βactin* (For: TGTCACCAACTGGGACGATA, Rev: GGGGTGTTGAAGGTCTCAAA). Human *TSHR* (For: AAGCTGGGGATGCGTTGAAT, Rev: CGGGGGACGTTCAGTTTGTA); Human *TBP* (For: ACAACAGCCTGCCACCTTA, Rev: GGGTCAGTCCAGTGCCATA). Human data were normalized to *TBP* expression.

scRNA-seq

TA and EOMss were dissociated as described above. After dissociation, cells were isolated by FACS after incubation with DAPI (D9542, Sigma-Aldrich) to obtain a cell suspension without dead cells and debris. scRNA-seq was performed using Chromium Next GEM Single Cell

3`Gene Expression V3 kit (10X Genomics) following the manufacturer's protocol. Sequencing was performed on Illumina NexSeq 550 system with High Output Kit v2.5 (75 Cycles, Illumina 20024906). Sample demultipexing, cell calling, transcript mapping, and gene expression counting were conducted with the Cell Ranger Software Suite v4.0.0. Sequence reads were aligned over a *Rattus norvegicus* reference genome build from Ensembl sources (EMBL-EBI, Rnor v6.0). Between-sample sequencing depth were adjusted by downsampling (Cell Ranger aggregate) and standardized to 17,253 confidentially mapped barcoded reads per cell. Clustering and data reduction were computed with Cell Ranger v4.0. A first linear dimension reduction by principal component analysis (PCA) was calculated to build a k-NN neighborhood graph enabling clustering and low-space embedding. t-SNE low-dimensionality projections were calculated on the 10 first PCA components, with a perplexity of 30 and a theta factor of 0.5. Cell clusters were determined by the Louvain Modularity algorithm with default parameters. All secondary analyses, including data visualization, cell cluster labelling, and differential expression testing were performed with the Loupe Cell Browser v5.0.

Functional tests

Maximal force was assessed by forelimb grip strength test. Repetitions of four measurements for each rat were measured by using a Bioseb grip device and the highest value was considered. Treadmill test was performed after 2 weeks of acclimation and training. The exhaustion test was performed by slowly increasing the speed of 2 cm/sec every 2 min starting from 5 cm/sec. Rats were removed from the treadmill if they remained immobile at the bottom of the treadmill for more than 20 s despite being encouraged to continue the exercise. The duration of the test was recorded for each rat and presented as exhaustion time.

Statistical analysis

Experiments were performed with a minimum of three biological replicates and results are presented as mean ± SEM. In every graph, each dot represents a single biological replicate, and the *P* values are indicated. Each experiment was conducted on at least 3 independent biological distinct samples as indicated in the figure legends. Statistical significance was calculated by Mann–Whitney U test to compare control and experimental groups. Two-way analysis of variance (ANOVA) with Sidak's post-test was used to compare more than two groups of samples with two variables (for example, genotype and cross-sectional area in Fig. 6E). All statistical analysis and graphs were performed using GraphPad Prism Software (version 7.0). The results are considered significant when $P < 0.05$.

Supplementary Materials

Fig. S1 to S4.

Data file S1

References and Notes

1. A. P. Monaco, R. L. Neve, C. Colletti-Feener, C. J. Bertelson, D. M. Kurnit, L. M. Kunkel, Isolation of candidate cDNAs for portions of the Duchenne muscular dystrophy gene. *Nature* **323**, 646-650 (1986).
2. Q. Q. Gao, E. M. McNally, The Dystrophin Complex: Structure, Function, and Implications for Therapy. *Compr Physiol* **5**, 1223-1239 (2015).
3. F. Relaix, M. Bencze, M. J. Borok, A. Der Vartanian, F. Gattazzo, D. Mademtzoglou, S. Perez-Diaz, A. Prola, P. C. Reyes-Fernandez, A. Rotini, t. Taglietti, Perspectives on skeletal muscle stem cells. *Nat Commun* **12**, 692 (2021).
4. Y. Echigoya, KR. Lim, A. Nakamura, T. Yokota, Multiple exon skipping in the Duchenne muscular dystrophy hot spots: Prospects and challenges. *Journal of personalized medicine*. 7;8(4):41 (2018).
5. V. Taglietti, K. Kefi, I. Bronisz-Budzynska, B. Mirciloglu, M. Rodrigues, N. Cardone, F. Coulpier, B. Periou, C. Gentil, M. Goddard, F. J. Authier, F. Pietri-Rouxel, E. Malfatti, P. Lafuste, L. Tiret, F. Relaix, Duchenne muscular dystrophy trajectory in R-DMDdel52 preclinical rat model identifies COMP as biomarker of fibrosis. *Acta Neuropathol Commun* **10**, 60 (2022).
6. H. J. Kaminski, M. al-Hakim, R. J. Leigh, M. B. Katirji, R. L. Ruff, Extraocular muscles are spared in advanced Duchenne dystrophy. *Ann Neurol* **32**, 586-588 (1992).
7. T. S. Khurana, R. A. Prendergast, H. S. Alameddine, F. M. Tome, M. Fardeau, K. Arahata, H. Sugita, L. M. Kunkel, Absence of extraocular muscle pathology in

Duchenne's muscular dystrophy: role for calcium homeostasis in extraocular muscle sparing. *J Exp Med* **182**, 467-475 (1995).
8. A. Hernandez-Segura, J. Nehme, M. Demaria, Hallmarks of Cellular Senescence. *Trends Cell Biol* **28**, 436-453 (2018).
9. D. Munoz-Espin, M. Serrano, Cellular senescence: from physiology to pathology. *Nat Rev Mol Cell Biol* **15**, 482-496 (2014).
10. A. Bernadotte, V. M. Mikhelson, I. M. Spivak, Markers of cellular senescence. Telomere shortening as a marker of cellular senescence. *Aging (Albany NY)* **8**, 3-11 (2016).
11. C. M. Dungan, B. D. Peck, R. G. Walton, Z. Huang, M. M. Bamman, P. A. Kern, C. A. Peterson, In vivo analysis of gammaH2AX+ cells in skeletal muscle from aged and obese humans. *FASEB J* **34**, 7018-7035 (2020).
12. C. Wang, D. Jurk, M. Maddick, G. Nelson, C. Martin-Ruiz, T. von Zglinicki, DNA damage response and cellular senescence in tissues of aging mice. *Aging Cell* **8**, 311-323 (2009).
13. S. Neumann, W. Huang, S. Titus, G. Krause, G. Kleinau, A. T. Alberobello, W. Zheng, N. T. Southall, J. Inglese, C. P. Austin, F. S. Celi, O. Gavrilova, C. J. Thomas, B. M. Raaka, M. C. Gershengorn, Small-molecule agonists for the thyrotropin receptor stimulate thyroid function in human thyrocytes and mice. *Proc Natl Acad Sci U S A* **106**, 12471-12476 (2009).
14. B. Rapoport, G. D. Chazenbalk, J. C. Jaume, S. M. McLachlan, The thyrotropin (TSH) receptor: interaction with TSH and autoantibodies. *Endocr Rev* **19**, 673-716 (1998).
15. L. Persani, G. Gelmini, F. Marelli, P. Beck-Peccoz, M. Bonomi, Syndromes of resistance to TSH. *Ann Endocrinol (Paris)* **72**, 60-63 (2011).
16. Y. D. Chu, C. T. Yeh, The Molecular Function and Clinical Role of Thyroid Stimulating Hormone Receptor in Cancer Cells. *Cells* **9**, (2020).
17. G. R. Williams, Extrathyroidal expression of TSH receptor. *Ann Endocrinol (Paris)* **72**, 68-73 (2011).
18. R. H. Alasbahi, M. F. Melzig, Forskolin and derivatives as tools for studying the role of cAMP. *Pharmazie* **67**, 5-13 (2012).
19. S. Schiaffino, A. C. Rossi, V. Smerdu, L. A. Leinwand, C. Reggiani, Developmental myosins: expression patterns and functional significance. *Skelet Muscle* **5**, 22 (2015).
20. Y. Zhou, D. Liu, H. J. Kaminski, Myosin heavy chain expression in mouse extraocular muscle: more complex than expected. *Invest Ophthalmol Vis Sci* **51**, 6355-6363 (2010).
21. S. Fraterman, U. Zeiger, T. S. Khurana, M. Wilm, N. A. Rubinstein, Quantitative proteomics profiling of sarcomere associated proteins in limb and extraocular muscle allotypes. *Mol Cell Proteomics* **6**, 728-737 (2007).
22. D. Kjellgren, LE. Thornell, J. Andersen, F. Pedrosa-Domellöf, Myosin heavy chain isoforms in human extraocular muscles. *Invest Ophthalmol Vis Sci*. 44(4):1419-25 (2003).
23. M. T. Budak, S. Bogdanovich, M. H. Wiesen, O. Lozynska, T. S. Khurana, N. A. Rubinstein, Layer-specific differences of gene expression in extraocular muscles identified by laser-capture microscopy. *Physiol Genomics* **20**, 55-65 (2004).
24. D. Kjellgren, L. E. Thornell, J. Andersen, F. Pedrosa-Domellof, Myosin heavy chain isoforms in human extraocular muscles. *Invest Ophthalmol Vis Sci* **44**, 1419-1425 (2003).
25. N. A. Rubinstein, J. F. Hoh, The distribution of myosin heavy chain isoforms among rat extraocular muscle fiber types. *Invest Ophthalmol Vis Sci* **41**, 3391-3398 (2000).

26. A. B. Rubenstein, G. R. Smith, U. Raue, G. Begue, K. Minchev, F. Ruf-Zamojski, V. D. Nair, X. Wang, L. Zhou, E. Zaslavsky, T. A. Trappe, S. Trappe, S. C. Sealfon, Single-cell transcriptional profiles in human skeletal muscle. *Sci Rep* **10**, 229 (2020).
27. B. Evano, D. Gill, I. Hernando-Herraez, G. Comai, T. M. Stubbs, P. H. Commere, W. Reik, S. Tajbakhsh, Transcriptome and epigenome diversity and plasticity of muscle stem cells following transplantation. *PLoS Genet* **16**, e1009022 (2020).
28. D. M. Noden, P. Francis-West, The differentiation and morphogenesis of craniofacial muscles. *Dev Dyn* **235**, 1194-1218 (2006).
29. S. Neumann, E. A. Nir, E. Eliseeva, W. Huang, J. Marugan, J. Xiao, A. E. Dulcey, M. C. Gershengorn, A selective TSH receptor antagonist inhibits stimulation of thyroid function in female mice. *Endocrinology* **155**, 310-314 (2014).
30. A. Moustogiannis, A. Philippou, O. Taso, E. Zevolis, M. Pappa, A. Chatzigeorgiou, M. Koutsilieris, The Effects of Muscle Cell Aging on Myogenesis. *Int J Mol Sci* **22**, (2021).
31. A. Ankala, J. N. Kohn, A. Hegde, A. Meka, C. L. Ephrem, S. H. Askree, S. Bhide, M. R. Hegde, Aberrant firing of replication origins potentially explains intragenic nonrecurrent rearrangements within genes, including the human DMD gene. *Genome Res* **22**, 25-34 (2012).
32. P. Stuelsatz, A. Shearer, Y. Li, L. A. Muir, N. Ieronimakis, Q. W. Shen, I. Kirillova, Z. Yablonka-Reuveni, Extraocular muscle satellite cells are high performance myo-engines retaining efficient regenerative capacity in dystrophin deficiency. *Dev Biol* **397**, 31-44 (2015).
33. H. Sugihara, N. Teramoto, K. Nakamura, T. Shiga, T. Shirakawa, M. Matsuo, M. Ogasawara, I. Nishino, T. Matsuwaki, M. Nishihara, K. Yamanouchi, Cellular senescence-mediated exacerbation of Duchenne muscular dystrophy. *Sci Rep* **10**, 16385 (2020).
34. L. V. Young, W. Morrison, C. Campbell, E. C. Moore, M. G. Arsenault, A. G. Dial, S. Ng, C. A. Bellissimo, C. G. R. Perry, V. Ljubicic, A. P. Johnston, Loss of dystrophin expression in skeletal muscle is associated with senescence of macrophages and endothelial cells. *Am J Physiol Cell Physiol* **321**, C94-C103 (2021).
35. V. Gorgoulis, P. D. Adams, A. Alimonti, D. C. Bennett, O. Bischof, C. Bishop, J. Campisi, M. Collado, K. Evangelou, G. Ferbeyre, J. Gil, E. Hara, V. Krizhanovsky, D. Jurk, A. B. Maier, M. Narita, L. Niedernhofer, J. F. Passos, P. D. Robbins, C. A. Schmitt, J. Sedivy, K. Vougas, T. von Zglinicki, D. Zhou, M. Serrano, M. Demaria, Cellular Senescence: Defining a Path Forward. *Cell* **179**, 813-827 (2019).
36. H. Y. Choi, H. Jeon, J. W. Yang, J. H. Ahn, J. H. Jung, Thyroid-Stimulating Hormone Receptor Expression on Primary Cultured Human Extraocular Muscle Myoblasts. *Curr Eye Res* **43**, 1484-1488 (2018).
37. M. Giménez-Barcons, R . Colobran, A. Gómez-Pau, A. Marín-Sánchez, A. Casteràs, G. Obiols, R. Abella, J. Fernández-Doblas, M. Tonacchera, A. Lucas-Martín, R. Pujol-Borrell, Graves' disease TSHR-stimulating antibodies (TSAbs) induce the activation of immature thymocytes: a clue to the riddle of TSAbs generation?. *The Journal of Immunology*. 1;194(9):4199-206 (2015).
38. B. Salehi, M. Staniak, K. Czopek, A. Stępień, K. Dua, R. Wadhwa, D. Kumar Chellappan, O. Sytar, M. Brestic, N. Ganesh Bhat, The therapeutic potential of the labdane diterpenoid forskolin. *Applied Sciences* **9**, 4089 (2019).
39. P. Sousa-Victor, E. Perdiguero, P. Munoz-Canoves, Geroconversion of aged muscle stem cells under regenerative pressure. *Cell Cycle* **13**, 3183-3190 (2014).
40. P. Sousa-Victor, S. Gutarra, L. Garcia-Prat, J. Rodriguez-Ubreva, L. Ortet, V. Ruiz-Bonilla, M. Jardi, E. Ballestar, S. Gonzalez, A. L. Serrano, E. Perdiguero, P. Munoz-

Canoves, Geriatric muscle stem cells switch reversible quiescence into senescence. *Nature* **506**, 316-321 (2014).
41. L. Garcia-Prat, M. Martinez-Vicente, E. Perdiguero, L. Ortet, J. Rodriguez-Ubreva, E. Rebollo, V. Ruiz-Bonilla, S. Gutarra, E. Ballestar, A. L. Serrano, M. Sandri, P. Munoz-Canoves, Autophagy maintains stemness by preventing senescence. *Nature* **529**, 37-42 (2016).
42. M. P. Godard, B. A. Johnson, S. R. Richmond, Body composition and hormonal adaptations associated with forskolin consumption in overweight and obese men. *Obes Res* **13**, 1335-1343 (2005).
43. S. Henderson, B. Magu, C. Rasmussen, S. Lancaster, C. Kerksick, P. Smith, C. Melton, P. Cowan, M. Greenwood, C. Earnest, A. Almada, P. Milnor, T. Magrans, R. Bowden, S. Ounpraseuth, A. Thomas, R. B. Kreider, Effects of coleus forskohlii supplementation on body composition and hematological profiles in mildly overweight women. *J Int Soc Sports Nutr* **2**, 54-62 (2005).
44. C. Nishijima, T. Chiba, Y. Sato, K. Umegaki, Nationwide Online Survey Enables the Reevaluation of the Safety of Coleus forskohlii Extract Intake Based on the Adverse Event Frequencies. *Nutrients* **11**, (2019).
45. H. L. Loftus, K. J. Astell, M. L. Mathai, X. Q. Su, Coleus forskohlii Extract Supplementation in Conjunction with a Hypocaloric Diet Reduces the Risk Factors of Metabolic Syndrome in Overweight and Obese Subjects: A Randomized Controlled Trial. *Nutrients* **7**, 9508-9522 (2015).

ACKNOWLEDGEMENT

We thank the "Institut Clinique de la Souris" – PHENOMIN for establishment of the DMD rat #188 mutant line. We thank Audrey Sophie, Lucy Foucher and Laurent Guillaud for animal care; Adeline Henry and Nathalie Didier for the optimization of the panel for satellite cell FACS sorting; Jules Gilet for help with bioinformatics analysis and the French Institute of Bioinformatics for providing computational resources. We also thank Cyril Gitiaux for his help in the acquisition of clinical samples of extraocular muscles. Editorial services were provided by Nancy R. Gough (BioSerendipity, LLC, Elkridge, MD).

Funding: This work was supported by funding from the "Association Française contre les Myopathies" (AFM) via the TRANSLAMUSCLE I and II programs (Projects 19507 and 22946), the "Fondation pour la recherche médicale" (FRM, grants EQU20200301021 and SPF20170938733), the "Agence Nationale pour la Recherche" (ANR, grant SenoMuscle ANR-21-CE13-0006); Labex REVIVE (ANR-10-LABX-73).

Author contribution:

Conceptualization: VT, FR

Experimental design: VT, MG, FPR, PL, FR, LT

Performed experiments: VT, KK, LR, OB, NC, FC, SG, BDL, CH, MR, DBG, LT

Analyzed data: VT, KK, LR, OB, NC, FC, SG, BDL, CH, MR, DBG, FPR, CB, CF, EM, FJA, LT

Writing and editing: VT, LT, FR

Project supervision: PL, LT, FR

Funding acquisition: FPR, PT, FJA, CB, EM, LT, CF, FR

Competing interests:

VT and FR have a patent related to the data reported in this paper (#FR2108489). The other authors declare that they have no competing interests.

Data and materials availability:

All data associated with this study are present in the paper or the supplementary materials. scRNA-seq data have been uploaded on Gene Expression Omnibus (GEO) database (GSE205629). Materials in this study are available via material transfer agreement by contacting the corresponding author (frederic.relaix@inserm.fr)

Table 1. 10X Genomics scRNA-seq parameters

	Estimated number of cells	**Mean reads per cell**	**Median genes per cell**	**Number of reads**	**Valid barcodes**	**Sequencing saturation**
WT TA	**3,550**	133,326	695	473,307,648	97.7%	92.7%
DMD TA	**8,944**	56,705	629	507,170,789	97.1%	86.5%
WT EOMs	**1,917**	234,365	1,012	449,279,284	98.3%	93.1%
DMD EOMs	**3,093**	144,443	1,350	446,762,721	97.7%	89.7%

DMD, Duchenne Muscular Dystrophy; EOM, extraocular muscles; TA, tibialis anterior; WT, wild-type

Figure legends

Figure 1. Impaired regenerative potential in limb but not extraocular muscles in R-DMDdel52 rats

(**A**) H&E and Sirius red staining of tibialis anterior muscles from R-DMDdel52 (DMD) and WT rats at 12 months. Scale bar = 50 μm. (**B**) Quantification of fibrotic tissue deposition based on area stained by Sirius red (n=3). (**C**) H&E and Sirius red staining of EOMs from R-DMDdel52 (DMD) and WT rats at 12 months. Scale bar = 50 μm. (**D**) Quantification of fibrotic tissue deposition based on area stained by Sirius red (n=3). (**E**) Immunofluorescent staining for eMHC and laminin on tibialis anterior. Nuclei are stained by Hoechst. Scale bar = 20 μm. (**F**) Quantification of the percentage of eMHC-positive cells in TA from 3 to 4 rats of the indicated genotypes. (**G**) Immunofluorescent staining for eMHC and laminin on EOMs. Nuclei are stained by Hoechst. Scale bar = 20 μm. (**H**) Quantification of the percentage of eMHC-positive cells in EOMs from 3 rats of the indicated genotypes. (**I**) Representative immunofluorescence of tibialiss anterior for PAX7, Ki67, laminin, and Hoechst. Yellow squares indicate proliferating MuSCs ($PAX7^+$ and $Ki67^+$); grey squares highlight non-proliferating ($PAX7^+$ and $Ki67^-$) MuSCs. Scale bar = 10 μm. (**J**) Quantification of $PAX7^+$ cells per fiber from muscles from 3-6 rats of each genotype. (**K**) Quantification of the percentage of cells that are both $PAX7^+$ and $Ki67^+$ ($PAX7^+$:$Ki67^+$) from muscles from 3-5 rats of each genotype. (**L**) Representative immunofluorescence staining of EOMs for PAX7, Ki67, laminin, and Hoechst. Yellow squares indicate $PAX7^+$:$Ki67^+$ MuSCs. Scale bar = 10 μm. (**M**) Quantification of $PAX7^+$ cells per fiber from 3 rats of each genotype. (**N**) Quantification of the percentage of $PAX7^+$:$Ki67^+$ cells from muscles from 3 rats of each genotype. Data are presented as mean ± SEM; Mann–Whitney U test.

Figure 2. Impaired proliferative and differentiation potential of myoblasts isolated from R-DMDdel52 rat limb muscles

(**A-B**) Representative immunofluorescent staining for Ki67, MYOD, and nuclei of myoblasts cultured from tibialis anterior (A) and EOMs (B) from 3-week-old WT and R-DMDdel52 rats. (**C**) Quantification of the percentage of myoblasts (PAX7 and/or MYOD positive) that co-express the proliferation marker Ki67 from 3 rats of each genotype. (**D**) Immunofluorescence for sarcomeric myosins (MHC) and nuclei from tibialis anterior and EOMs cultured from 3-week-old rats of the indicated genotypes. (**E-F**) Analysis of fusion capacity by fusion index evaluation (E) and nuclei per myotube (F) using cells stained as in D of cells cultured from 3 rats of each genotype. (**G-H**) Representative immunofluorescence staining for Ki67, MYOD, and nuclei from myoblasts cultured from tibialis anterior (G) and EOMs (H) from 6-month-old rats. (**I**) Quantification of the percentage of $PAX7^+$ or $MYOD^+$:$Ki67^+$ cells in MuSCs cultured from 3 rats of each genotype. (**J**) Immunofluorescence for MHC and nuclei from tibialis anterior and EOMs. (**K-L**) Analysis of fusion capacity by fusion index (K) and nuclei per myotube (L) from images stained as in J of cells cultured from 3 rats of each genotype. (**M**) Representative immunofluorescence for EdU, PAX7 and MYOD (both green), and nuclei from myoblasts isolated from quadriceps muscles from 6-month-old rats and purified by FACS. (**N**) Percentage of cells that are positive for PAX7 and MYOD from cells stained as in M. (**O**) Quantification of percentage of proliferating (EdU^+) myoblasts from cells stained as in M. Data in both N and O were quantified from cells isolated from 3 rats of each genotype. (**P**) Representative immunofluorescence for MHC and nuclei of myoblasts differentiated in culture after isolation from quadriceps of 6-month-old rats and purification by FACS. Scale bar = 50 μm. (**Q**) Quantification of fusion index per field from cells stained as in P from cells isolated from 3 rats of each genotype.

Scale bars are 20 μm for all the pictures except for P. In A, B, G, H, and M, yellow arrowheads indicate MYOD^{+}:Ki67^{+} myoblasts; light blue arrowheads indicate MYOD^{+}:Ki67^{-} cells. Data presented as mean ± SEM; Mann–Whitney U test.

Figure 3. scRNA-seq analysis of limb muscles and EOMs from 12-month-old wild-type and R-DMDdel52 rats

(**A**) t-SNE plot of muscle-resident cell populations in TA WT and R-DMDdel52 rats. (**B**) t-SNE and violin plots showing *Cdkn1a* and *Cdkn2a* expression. (**C-H**) Representative immunofluorescence and quantification of PAX7, laminin, and Hoechst with P16 (C, F), P21 (D, G), or γH2AX (E, H) in TA from at 12-month-old rats of the indicated genotypes. Yellow triangles highlight PAX7^{+} MuSCs. Scale bars = 10 μm. Quantification of percentage of cells that are positive for both PAX7 and P16, P21, or γH2AX was performed on muscle sections from 3-4 rats of each genotype. (**I**) scRNAseq-based t-SNE plot representing muscle-resident cell populations of TA and EOMs showing the expression of *Pax7, Pitx2, Cdkn1a, Cdkn2a*, and *Tshr*. Blue rectangles indicate MuSC clusters. (**J**) Violin plots showing scRNA-seq-based expression of the indicated genes. (**K**) RT-qPCR analysis of *Cdkn1a, Cdkn2a*, and *Tshr* in limb- and EOM-derived myoblasts, normalized to their expression in WT limb myoblasts. Transcripts were assessed in myoblasts isolated from 3-5 rats of each genotype. Data presented as mean ± SEM; Mann–Whitney U test.

Figure 4. Modulating TSHR signaling in cultured DMD myoblasts impacts their senescence and regenerative capacities

(**A**) Representative immunofluorescence for TSHR (red), PAX7:MYOD (both green), and nuclei (Hoechst, blue) of 3-month-old myoblasts isolated from EOMs and TA muscles. Merged images are shown. Scale bars = 20 μm. (**B**) Representative immunofluorescence of EdU (red), PAX7:MYOD (both green), and nuclei (Hoechst, blue) of EOM-derived myoblasts treated with vehicle (DMSO), ML224, or ML224 and forskolin (ML224 + FS). Scale bars = 20 μm. (**C**) Quantification of percentage of proliferating PAX7:MYOD cells stained as in B from EOMs isolated from 3 wild-type rats. (**D**) RT-qPCR analysis of *Cdkn1a* and *Cdkn2a* in EOM-derived myoblasts exposed to vehicle, ML224, or ML224 + FS from EOMs isolated from 3 wild-type rats. (**E-G**) Analysis of fusion capacity of myoblasts derived from EOM. Immunofluorescence staining for MHC and nuclei of differentiated myotubes (E). Scale bars = 20 μm. Fusion index evaluation (F) and number of nuclei per myotube (G) were calculated from EOMs isolated from 3 wild-type rats. (**H**) Representative immunofluorescence of PAX7:MYOD (both green), Ki67, and nuclei (Hoechst, blue) of limb-derived myoblasts treated with vehicle or forskolin. Scale bars = 20 μm. (**I**) Quantification of percentage of proliferating PAX7:MYOD cells stained as in H from TAs of 4 independent wild-type and R-DMDdel52 rats. (**J**) RT-qPCR analysis of *Cdkn1a* and *Cdkn2a* in limb-derived myoblasts treated with vehicle or forskolin from TAs of 4 independent wild-type and R-DMDdel52 rats. (**K**) Analysis of fusion capacity of myoblasts derived from TA muscles. Representative immunofluorescence for MHC and nuclei of differentiated myotubes treated with vehicle or forskolin (K). Scale bars = 200 μm. Fusion index evaluation was calculated from TAs of 4 independent wild-type and R-DMDdel52 rats. Data presented as mean ± SEM are from TAs of 4 independent wild-type and R-DMDdel52 rats; Mann–Whitney U test.

Figure 5. Progressive loss of muscle regeneration capacity and premature senescence of MuSCs in patients with DMD.

(**A**) Immunostaining for eMHC and laminin on control and DMD human biopsies taken from patients at the indicated ages. Scale bars = 20 μm. (**B**) Quantification of the number of $eMHC^+$ myofibers per mm^2 from tissue stained as in A (Control n=12 tissue samples; DMD n=20 patient samples). (**C-D**) Representative immunofluorescence staining of DMD and control muscle biopsies for nuclei (Hoechst), laminin, and PAX7 with P16 (C) or γH2AX (D). Yellow triangles highlight PAX7+ MuSCs. Scale bars = 10 μm. (**E, F**) Quantification of percentage of $PAX7^+$ cells that were positive for P16 (E, Control n = 12; DMD = 20) or γH2AX (F, Control n = 12; DMD n = 15). (**G**) Representative immunostaining for TSHR (red), PAX7:MYOD (both green), and nuclei (Hoechst, blue) of human EOM and deltoid myoblasts after 2 days of culture. Merged images are shown. Scale bars = 10 μm. (**H**) RT-qPCR analysis of *TSHR* in human EOM and limb myoblasts from 3 independently prepared deltoid/EOM-derived myoblasts. (**I, J**) Representative immunofluorescence staining of PAX7:MYOD (both green), EdU (purple), and nuclei (Hoescht, blue) of human myoblasts isolated from EOMs (I) or limb muscles (J) treated with vehicle (DMSO) or ML224. Scale bars = 20 μm. (**K, L**) Quantification of $PAX7:MYOD^+EdU^+$ and $PAX7:MYOD^+/EdU^-$ myoblasts from human EOMs (K) or deltoid muscles (L) upon treatment with ML224 or vehicle (DMSO). Data are shown for 3 independently prepared deltoid/EOM-derived myoblasts. Data presented as mean ± SEM; Mann–Whitney U test.

Figure 6. Systemic treatment of R-DMDdel52 rats with forskolin improves muscle performance and regenerative capacities.

(**A**) Scheme of forskolin (FS) treatment, including 2 months of injections followed by one month without injection after which the animals were euthanized (**B**) Grip test. (**C**) Exhaustion

time by treadmill. (**D**) H&E staining on TA. Scale bar 50 μm. (**E**) Graph showing the CSA distribution in TA. Statistical analysis marked by $ is calculated between WT and DMD, while the one marked by # is evaluated between WT and DMD+FS (two-way ANOVA with Sidak's post-test, from 4 rats of each genotype and treatment). (**F**) Sirius Red staining of TA. Scale bar 50 μm. (**G**) Quantification of fibrosis seen in F from TAs of 4 independent wild-type and R-DMDdel52 rats treated with vehicle or forskolin. (**H**) Representative immunofluorescences of eMHC and laminin. Scale bar 20 μm. (**I**) Quantification of eMHC-positive regenerating myofibers from TAs of 4 independent wild-type and R-DMDdel52 rats treated with vehicle or forskolin. (**J**) Representative co-immunofluorescence of PAX7, Ki67, LAMININ and nuclei on TA. White triangles highlight $PAX7^+$ MuSCs. Scale bar 10 μm. (**K**) Quantification of proliferating (Ki67+) MuSCs (PAX7+) from TAs of 4 independent wild-type and R-DMDdel52 rats treated with vehicle or forskolin. (**L**) Representative co-immunofluorescence of PAX7, P16, laminin and Hoechst. White triangles highlight $PAX7^+$ MuSCs. Scale bar 10 μm. (**M**) Quantification of MuSCs (PAX7+) expressing P16 from TAs of 4 independent wild-type and R-DMDdel52 rats treated with vehicle or forskolin. (**N**) Immunofluorescence of PAX7:MYOD, Ki67 and nuclei. White triangles highlight $Ki67^+$ myoblasts, while yellow triangles point Ki67- myoblasts. Scale bar 10 μm. (**O**) Immunofluorescence of MHC and Hoechst. Scale bar 20 μm. (**P**) Quantification of $PAX7:MYOD^+/Ki67^+$ from myoblasts isolated from quadriceps of 4 independent wild-type and R-DMDdel52 rats treated with vehicle or forskolin. (**Q**) Fusion index of differentiated myoblasts isolated from quadriceps of 4 independent wild-type and R-DMDdel52 rats treated with vehicle or forskolin. Data presented as means ± SEM; Mann–Whitney U test.

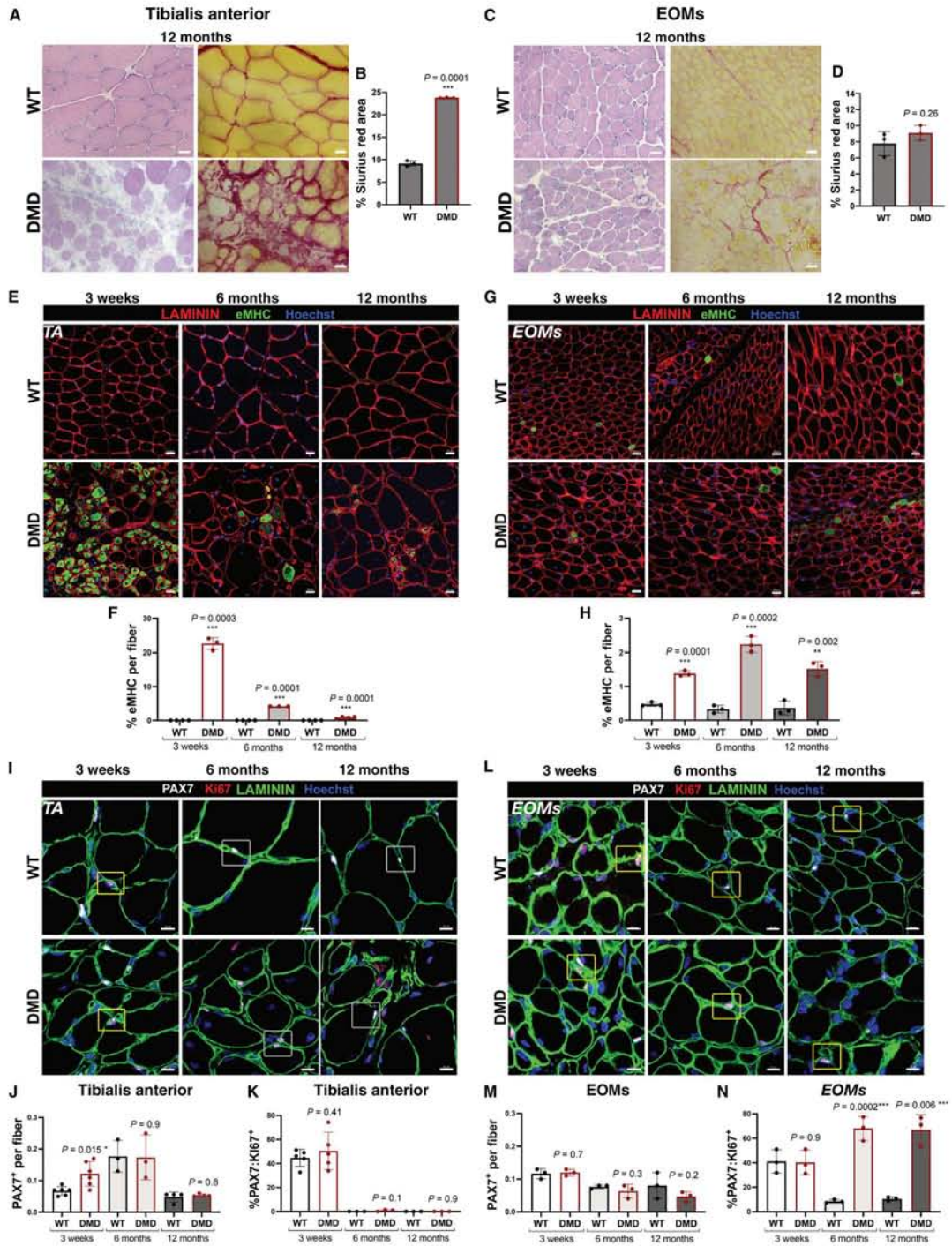
A
Tibialis anterior
12 months
WT
DMD
B
% Siurius red area
P = 0.0001
***
WT
DMD
C
EOMs
12 months
WT
DMD
D
% Siurius red area
P = 0.26
WT
DMD
E
3 weeks
6 months
12 months
LAMININ eMHC Hoechst
TA
WT
DMD
F
% eMHC per fiber
P = 0.0003
***
P = 0.0001
***
P = 0.0001
***
WT DMD WT DMD WT DMD
3 weeks
6 months
12 months
G
3 weeks
6 months
12 months
LAMININ eMHC Hoechst
EOMs
WT
DMD
H
% eMHC per fiber
P = 0.0001
***
P = 0.0002
***
P = 0.002
**
WT DMD WT DMD WT DMD
3 weeks
6 months
12 months
I
3 weeks
6 months
12 months
PAX7 Ki67 LAMININ Hoechst
TA
WT
DMD
L
3 weeks
6 months
12 months
PAX7 Ki67 LAMININ Hoechst
EOMs
WT
DMD
J
Tibialis anterior
PAX7+ per fiber
P = 0.015
*
P = 0.9
P = 0.8
WT DMD WT DMD WT DMD
3 weeks
6 months
12 months
K
Tibialis anterior
%PAX7:KI67+
P = 0.41
P = 0.1
P = 0.9
WT DMD WT DMD WT DMD
3 weeks
6 months
12 months
M
EOMs
PAX7+ per fiber
P = 0.7
P = 0.3
P = 0.2
WT DMD WT DMD WT DMD
3 weeks
6 months
12 months
N
EOMs
%PAX7:KI67+
P = 0.9
P = 0.0002
***
P = 0.006
***
WT DMD WT DMD WT DMD
3 weeks
6 months
12 months

FIGURE 1

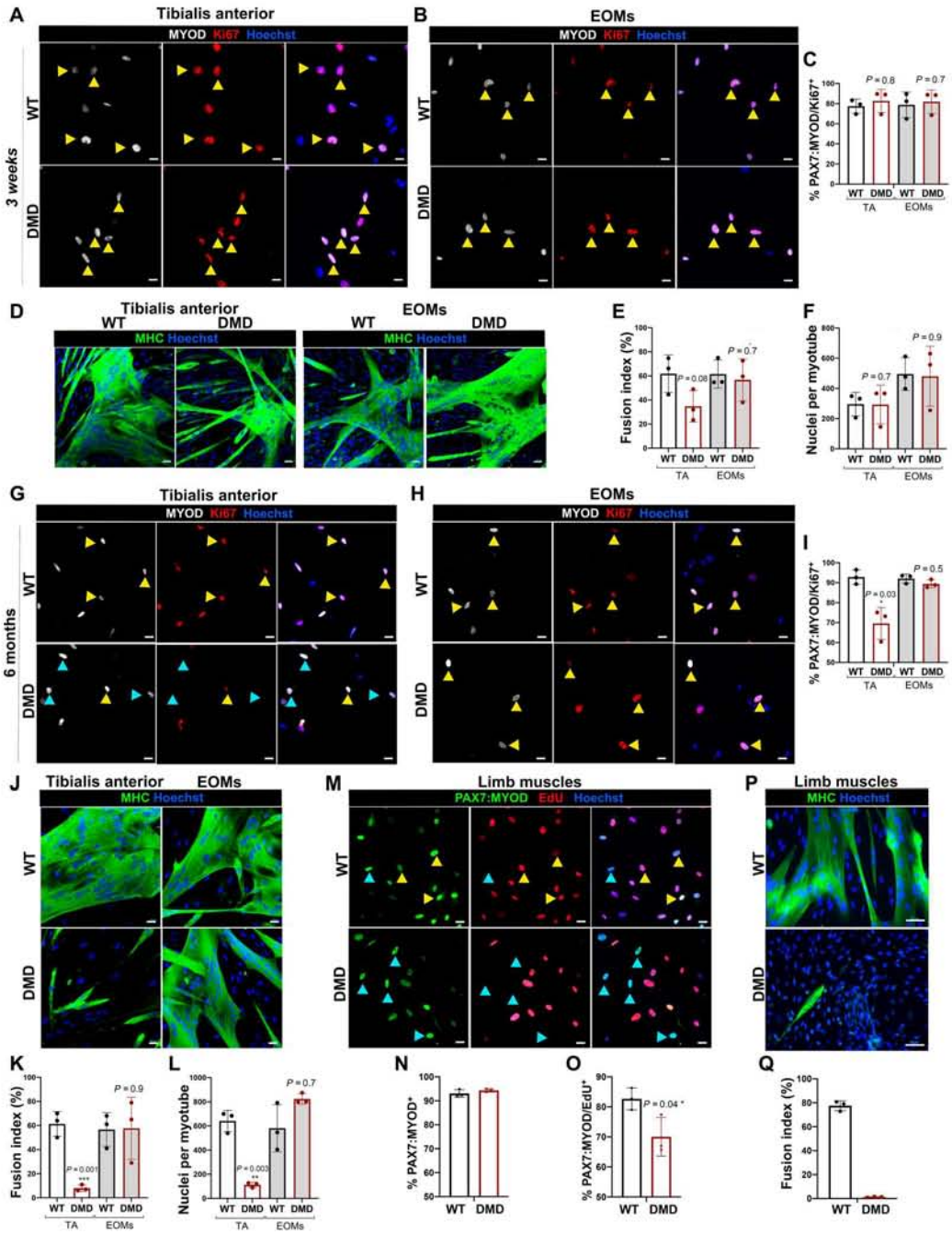
A
Tibialis anterior
MYOD Ki67 Hoechst
3 weeks
WT
DMD
B
EOMs
MYOD Ki67 Hoechst
C
% PAX7:MYOD/Ki67+
P = 0.8
P = 0.7
WT DMD WT DMD
TA EOMs
D
Tibialis anterior
EOMs
WT DMD
MHC Hoechst
E
Fusion index (%)
P = 0.08
P = 0.7
F
Nuclei per myotube
P = 0.7
P = 0.9
G
Tibialis anterior
MYOD Ki67 Hoechst
6 months
H
EOMs
I
% PAX7:MYOD/Ki67+
P = 0.03
P = 0.5
J
Tibialis anterior
EOMs
MHC Hoechst
M
Limb muscles
PAX7:MYOD EdU Hoechst
P
Limb muscles
MHC Hoechst
K
Fusion index (%)
P = 0.001
P = 0.9
L
Nuclei per myotube
P = 0.003
P = 0.7
N
% PAX7:MYOD+
O
% PAX7:MYOD/EdU+
P = 0.04 *
Q
Fusion index (%)

FIGURE 2

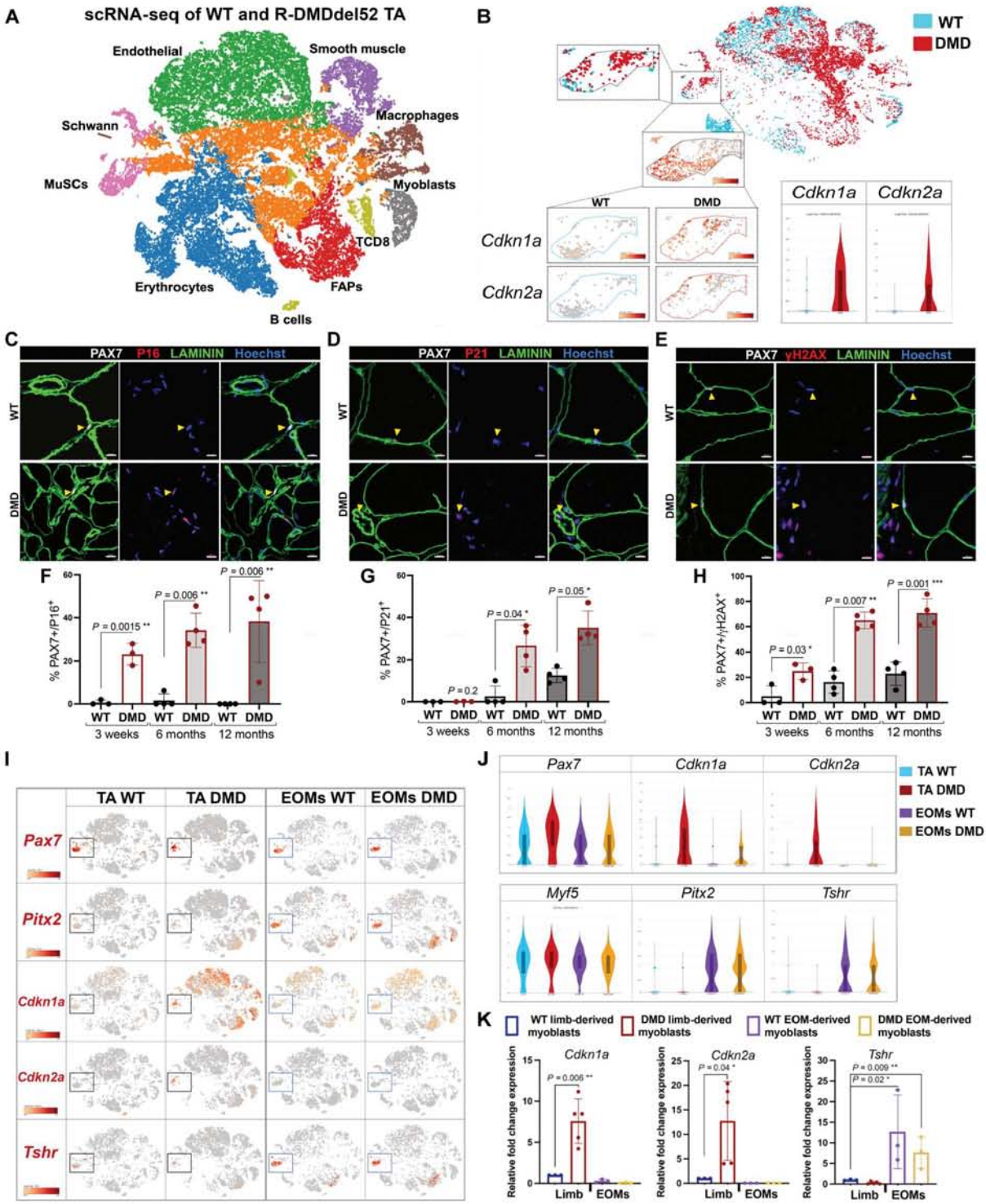
A
scRNA-seq of WT and R-DMDdel52 TA
Endothelial
Smooth muscle
Schwann
Macrophages
MuSCs
Myoblasts
TCD8
Erythrocytes
FAPs
B cells
B
WT
DMD
Cdkn1a
Cdkn2a
C
PAX7 P16 LAMININ Hoechst
D
PAX7 P21 LAMININ Hoechst
E
PAX7 γH2AX LAMININ Hoechst
F
% PAX7+/P16+
P = 0.0015 **
P = 0.006 **
P = 0.006 **
G
% PAX7+/P21+
P = 0.2
P = 0.04 *
P = 0.05 *
H
% PAX7+/γH2AX+
P = 0.03 *
P = 0.007 **
P = 0.001 ***
WT DMD WT DMD WT DMD
3 weeks 6 months 12 months
I
TA WT
TA DMD
EOMs WT
EOMs DMD
Pax7
Pitx2
Cdkn1a
Cdkn2a
Tshr
J
Pax7
Cdkn1a
Cdkn2a
Myf5
Pitx2
Tshr
TA WT
TA DMD
EOMs WT
EOMs DMD
K
WT limb-derived myoblasts
DMD limb-derived myoblasts
WT EOM-derived myoblasts
DMD EOM-derived myoblasts
Relative fold change expression
Cdkn1a
P = 0.006 **
Cdkn2a
P = 0.04 *
Tshr
P = 0.009 **
P = 0.02 *
Limb
EOMs

FIGURE 3

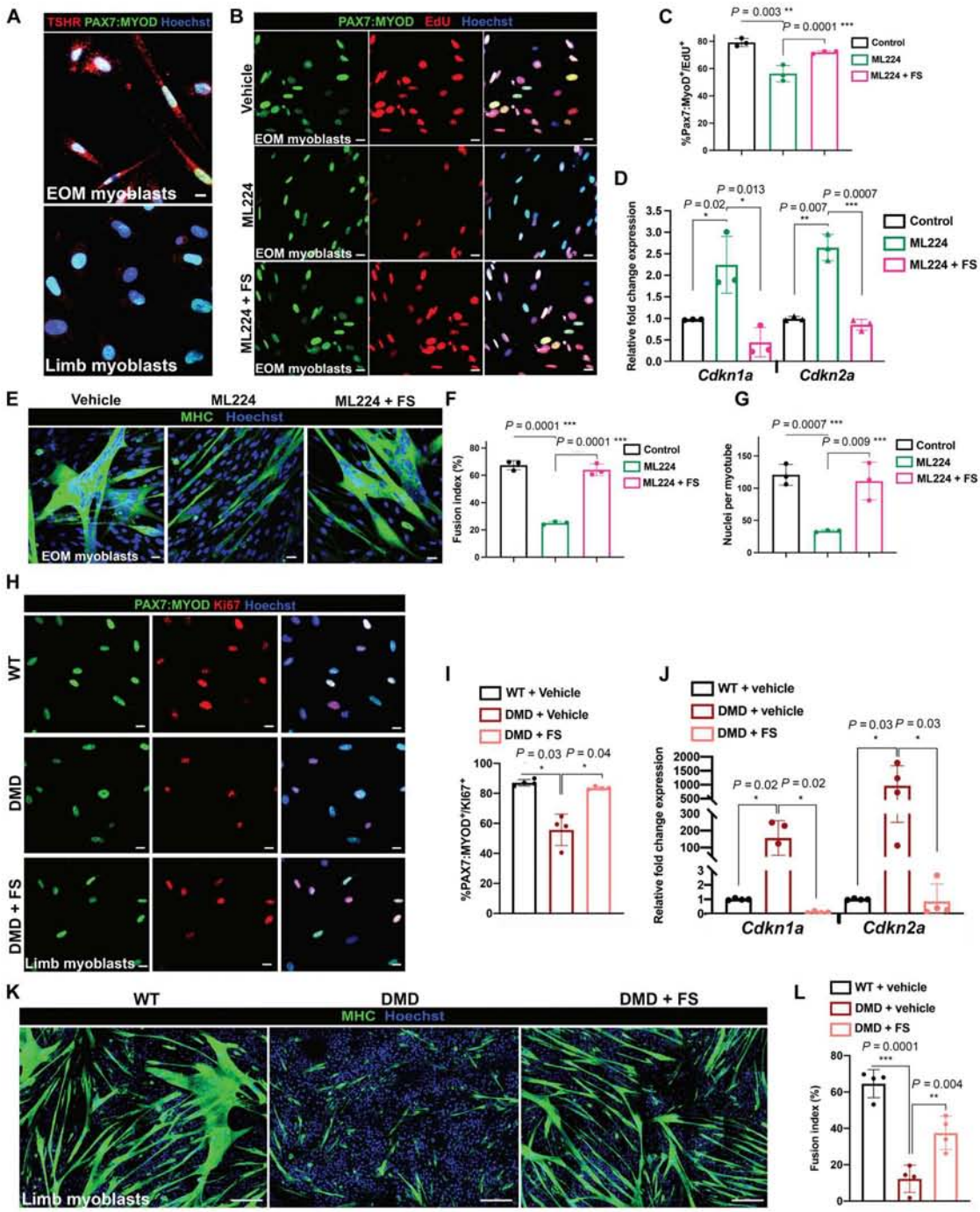
A
TSHR PAX7:MYOD Hoechst
EOM myoblasts
Limb myoblasts
B
PAX7:MYOD EdU Hoechst
Vehicle
ML224
ML224 + FS
EOM myoblasts
C
P = 0.003 **
P = 0.0001 ***
%Pax7:MyoD+/EdU+
Control
ML224
ML224 + FS
D
P = 0.02
P = 0.013
P = 0.007
P = 0.0007
Relative fold change expression
Cdkn1a
Cdkn2a
E
Vehicle
ML224
ML224 + FS
MHC Hoechst
EOM myoblasts
F
P = 0.0001 ***
P = 0.0001 ***
Fusion index (%)
G
P = 0.0007 ***
P = 0.009 ***
Nuclei per myotube
H
PAX7:MYOD Ki67 Hoechst
WT
DMD
DMD + FS
Limb myoblasts
I
WT + Vehicle
DMD + Vehicle
DMD + FS
P = 0.03
P = 0.04
%PAX7:MYOD+/KI67+
J
WT + vehicle
DMD + vehicle
DMD + FS
P = 0.02
P = 0.02
P = 0.03
P = 0.03
Relative fold change expression
Cdkn1a
Cdkn2a
K
WT
DMD
DMD + FS
MHC Hoechst
Limb myoblasts
L
WT + vehicle
DMD + vehicle
DMD + FS
P = 0.0001
P = 0.004
Fusion index (%)

FIGURE 4

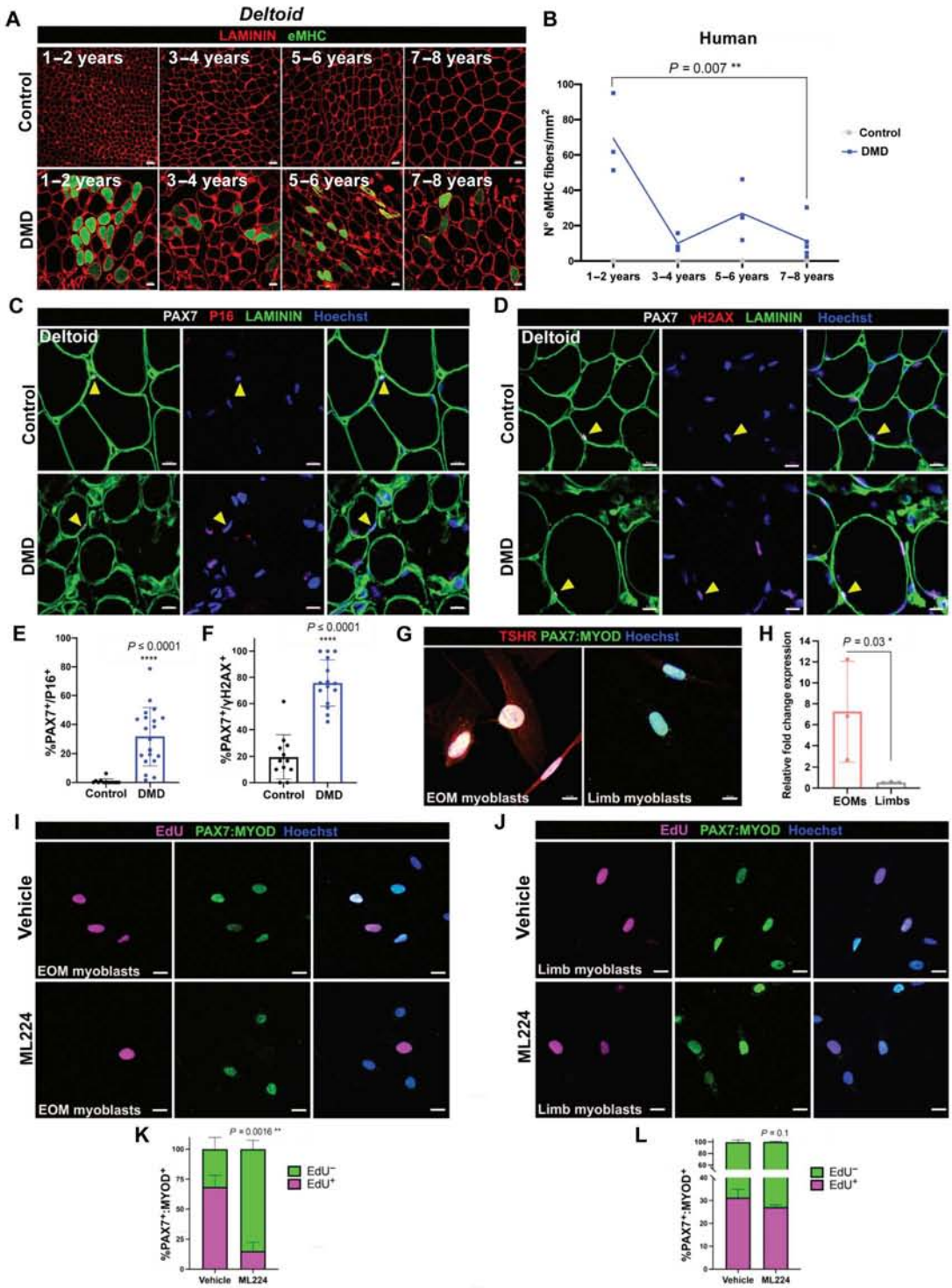
A
Deltoid
LAMININ eMHC
1–2 years
3–4 years
5–6 years
7–8 years
Control
DMD
B
Human
P = 0.007 **
N° eMHC fibers/mm²
Control
DMD
C
PAX7 P16 LAMININ Hoechst
Deltoid
D
PAX7 γH2AX LAMININ Hoechst
E
P ≤ 0.0001
%PAX7⁺/P16⁺
F
P ≤ 0.0001
%PAX7⁺/γH2AX⁺
G
TSHR PAX7:MYOD Hoechst
EOM myoblasts
Limb myoblasts
H
P = 0.03 *
Relative fold change expression
EOMs
Limbs
I
EdU PAX7:MYOD Hoechst
Vehicle
ML224
J
K
P = 0.0016 **
%PAX7⁺:MYOD⁺
EdU⁻
EdU⁺
L
P = 0.1

FIGURE 5

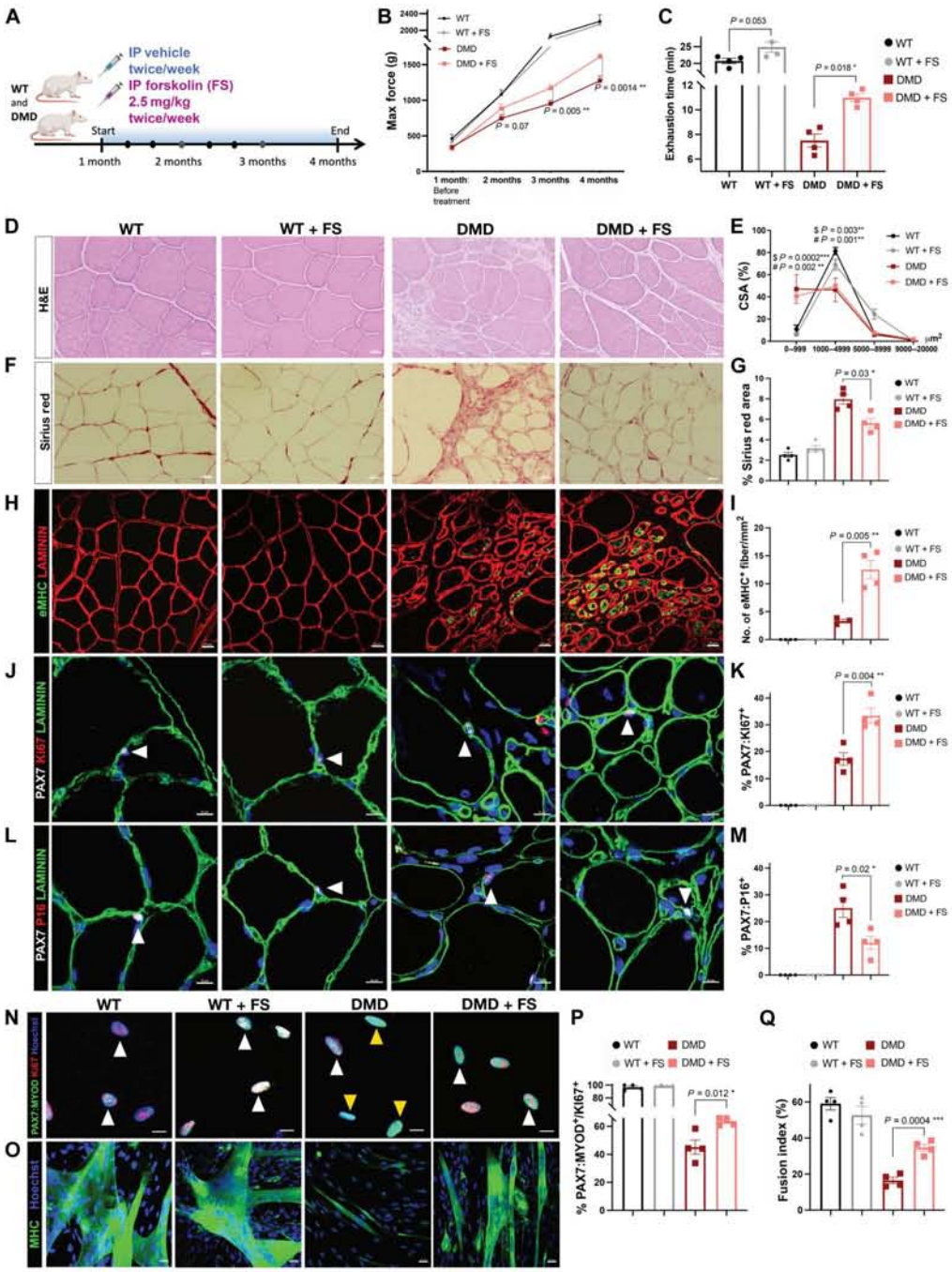
A
IP vehicle twice/week
IP forskolin (FS) 2.5 mg/kg twice/week
WT and DMD
Start
End
1 month
2 months
3 months
4 months
B
Max force (g)
WT
WT + FS
DMD
DMD + FS
P = 0.07
P = 0.005 **
P = 0.0014 **
1 month: Before treatment
2 months
3 months
4 months
C
Exhaustion time (min)
P = 0.053
P = 0.018 *
WT
WT + FS
DMD
DMD + FS
D
WT
WT + FS
DMD
DMD + FS
H&E
E
CSA (%)
$ P = 0.003**
# P = 0.001**
$ P = 0.0002***
# P = 0.002 **
µm²
0–999
1000–4999
5000–8999
9000–20000
F
Sirius red
G
% Sirius red area
P = 0.03 *
H
eMHC LAMININ
I
No. of eMHC⁺ fiber/mm²
P = 0.005 **
J
PAX7 KI67 LAMININ
K
% PAX7:KI67⁺
P = 0.004 **
L
PAX7 P16 LAMININ
M
% PAX7:P16⁺
P = 0.02 *
N
PAX7:MYOD KI67 Hoechst
O
MHC Hoechst
P
% PAX7:MYOD⁺/KI67⁺
P = 0.012 *
Q
Fusion index (%)
P = 0.0004 ***

FIGURE 6